



北京正负电子对撞机国家实验室

2001

北京**同步辐射**装置

用户科技论文集

(上册)

北京正负电子对撞机国家实验室办公室编印

序

2000-2001 运行年度, BSRF 的工作一直得到广大用户的极大支持和关爱, 使我们的工作又有长足的进展。同步辐射专用运行机时增加, 光源质量进一步改善, 课题管理更加完善, 研究领域有所扩展, 研究水平不断提高。经过多年的积累, 许多研究课题取得了丰硕的成果, 有的课题取得了重大突破, 一些具有创新性、高难度的课题也取得了不同程度的进展。

为了促进 BSRF 与国内、外科学家的交流合作, 也作为 BSRF 工作的鞭策。我们从 1997 年起收集用户和 BSRF 工作人员在 BSRF 上全部或部分实验发表的论文。每年编辑一册“北京同步辐射装置上的科学研究论文集”。2001 年在国内外学术杂志上发表论文 131 篇(不完全统计), 本论文集共收集用户论文 102 篇, 其中 SCI 收录 110 余篇, 影响因子 1—1.5 的 19 篇, 1.5—2.0 的 10 篇, 大于 2 的 8 篇。本论文集是 2000-2001 运行年度 BSRF 科研工作的缩影, 是广大用户和 BSRF 工作人员辛勤劳动和聪明才智的结晶。在此, 我们感谢为 BSRF 发展做出贡献的广大用户和 BSRF 工作人员。由于各种原因, 可能还有一些高水平的论文没有收集到“论文集”中, 我们谨向这些论文的作者表示深深的歉意。

另有部分文章已在“高能物理与核物理”2001 年增刊刊载, 为了避免重复, 本文集只登录文章目录, 原文请见高能物理与核物理(GAONENG WULI YU HEWULI)第 25 卷 增刊。

袁振洪

2001 年 4 月

北京同步辐射装置用户 2001 年科技论文目录

(上 册)

【EXAFS 实验站】

1. Local structure of NiTi nanocrystals studied by EXAFS and XRD 巨 新等 (1)
2. Preparation and photoluminescence of nanowire array and films of cadmium sulfide by electrodepositing in organic solvent 巨 新等 (3)
3. Evidence for change of the interfacially local structure of titanium oxide/bis[4, 4'-carboxy-2, 2'-bipyridine](thiocyanato)] ruthenium nanocomposite 巨 新等 (9)
4. 机械球磨非晶化的 XAFS 研究 刘 涛等 (12)
5. γ - Mo_2N 和分子筛负载的钼氮化物的结构表征 刘振林等 (17)
6. Mechanism of SO_2 Promotion for NO Reduction with NH_3 over Activated Carbon-Supported Vanadium Oxide Catalyst 朱珍平等 (22)
7. Symmetry dependence of X-ray absorption near-edge structure at the metal K edge of 3d transition metal compounds 吴白玉等 (33)
8. Experimental and theoretical XANES study of the effects of Fe-Mg solid solution in the enstatite-ferrosilite series 吴白玉等 (36)
9. Symmetry role on the pre-edge X-ray absorption fine structure at the metal K edge 吴白玉等 (39)
10. Hg L₃-edge Absorption Study of $\text{HgBa}_2\text{CuO}_{4-x}$ Superconductor 吴白玉等 (42)
11. Experimental and theoretical XANES and EXAFS study of tetra-ferriphlogopite Gabriele GIULI 等 (46)
12. On the change of electronic states at the Fermi level by Ce doping in the intermetallic LaRu_2 N.L.Saini 等 (56)
13. EXAFS study of molybdenum oxide on the structure Al_2O_3 ... Weiping Shi 等 (60)
14. Structures of surface-and bulk-dispersion phases of Ni/ Al_2O_3 蔡小海等 (63)
15. EXAFS study on the local atomic structures around iron in glycosylated Haemoglobin 吴忠华等 (66)
16. Structural Characteristics of Cerium Oxide Nanocrystals Prepared by the Microemulsion Method 张 静等 (73)
17. XANES study on the valence transitions in cerium oxide nanoparticles 张 静等 (79)
18. New observations on the optical properties of PPV/ TiO_2 nanocomposites 张 静等 (81)
19. Study on the optical properties of PPV/ TiO_2 nanocomposites 张 静等 (87)
20. Effect of cobalt promoter on Co-Mo-K/C catalysts used for mixed alcohol synthesis 李忠瑞等 (92)
21. Active carbon supported Mo-K catalysts used for alcohol synthesis 李忠瑞等 (102)
22. 活性炭担载的 Rh-Mo-K 合成醇催化剂 李忠瑞等 (109)
23. 硫化态 Co-Mo-K/AC 合成醇催化剂的 EXAFS 研究 李忠瑞等 (115)
24. 三氧化二铝含量对 $\text{Ni/Zr}_{0.4}\text{Ce}_{0.6}\text{O}_2\text{-Al}_2\text{O}_3$ 催化剂的 $\text{CH}_4\text{-CO}_2$ 重整反应性能影响 李春林等 (120)

25. 氧化铝负载高分散 γ - Mo_2N 的制备及其微观结构的 EXAFS 表征孟 明等 (124)
26. XAFS characterization on the active sites of Ni/ γ - Al_2O_3 catalysts for no-SCR by propene孟 明等 (128)
27. Synthesis of zincosilicate mordenite using citric acid as complexing agent董 梅等 (138)
28. Determination of double decker sandwich structured La-substituted chlorophyll a by EXAFS陶 冶等 (145)
29. A beam position monitor and slit combination for synchrotron radiation谢亚宁等 (147)
30. Monochromator development at 4W1B beamline of BSRF谢亚宁等 (151)
31. BERF XAFS 的新进展—全反射 XAFS 实验方法谢亚宁等 (155)
32. 不同方法制备的硫化态 K-Co-Mo 催化剂的 EXAFS 研究鲍 骏等 (158)
33. 不同热处理方式对超细粒子 K-Co-Mo 催化剂性能和结构的影响鲍 骏等 (164)

【真空紫外光谱实验站】

34. Eu^{3+} 和 Tb^{3+} 在 $\text{LnBaB}_9\text{O}_{16}$ 中的紫外和真空紫外发光性质杨 智等 (170)
35. $\text{SrB}_4\text{O}_7:\text{Pr}^{3+}$ 中 Pr^{3+} 的发光性质杨 智等 (176)
36. $\text{Gd}_2\text{O}_3(\text{Ce}^{3+}, \text{Eu}^{3+})$ 微晶中稀土离子间的级联能量传递魏亚光等 (180)

【光电子谱学实验站】

37. Growth and characterization of SrMoO_3 thin filmsH. H. Wang 等 (185)
38. 花四羧酸铈在 TiO_2 纳米晶膜上的光电转化性质王忠胜等 (191)
39. Self-assembly and photoelectric properties of cerium complexes with 3, 4, 9, 10-perylenetetra-carboxylic acid on nanocrystalline TiO_2 films王忠胜等 (197)
40. Ultrathin Pb film growth on Cu (111) studied by photoemission徐明春等 (205)
41. 乙烯在 $\text{Ru}(10\bar{1}0)$ 表面价带电子特性研究张建华等 (211)
42. $\text{C}_2\text{H}_2, \text{C}_2\text{H}_4$ 与 K 在 $\text{Ru}(10\bar{1}0)$ 表面上共吸附的 UPS 研究张建华等 (216)
43. Investigation of Bonding in Nano- SiO_2 by $\text{Si L}_{2,3}$ X-ray absorption Near-edge structure Spectroscopy吴白玉等 (220)
44. Oxygen 1s ELNES study of perovskites $(\text{Ca}, \text{Sr}, \text{Ba})\text{TiO}_3$ 吴白玉等 (226)
45. NEXAFS multiple scattering calculations of KO_2 M. Pedio 等 (229)
46. Resonant Photoemission of Bulk CeO_2 and Nano- CeO_2 Films买买提依明等 (232)
47. Investigation on the valence state of Ce atom in bulk and nanocrystal CeO_2 by x-ray absorption and photoemission奎热西等 (237)
48. 弧光放电原位清洗光学元件钱海杰等 (243)

【荧光分析实验站】

49. Compositional change in human enamel irradiated with MIR free electron laser刘年庆等 (246)
50. Synchrotron radiation XRF microprobe investigation of elemental distribution in femoral head slice with osteoporosis张元勋等 (249)
51. 南极菲尔德斯半岛六种藻类和地衣植物的 X 荧光分析沈显生等 (253)

52. 南极乔治王岛六种苔藓植物的 X 荧光分析沈显生等 (261)
53. 用同步光微束作激发源的 PSS 性能研究胡朝晖等 (268)
54. 同步辐射 X 射线荧光分析在植物微量元素分析中的应用康世秀等 (273)
55. Single fluid inclusion study by SRXRF microprobe黄宇营等 (278)
56. Study of human bone tumor slice by SRXRF microprobe黄宇营等 (281)
57. Beijing Synchrotron Radiation TXRF Facility and its Applications on Trace Element Study of Cells黄宇营等 (285)

Local structure of NiTi nanocrystals studied by EXAFS and XRD

Xin JU, Yixi SU

Institute of High Energy Physics, Chinese Academy of Sciences, Beijing 100039, P. R. China, Email: jux@alpha02.ihep.ac.cn

A series of NiTi nanocrystals with different annealing temperatures, prepared by sputtering method, were investigated by extended x-ray absorption fine structure (EXAFS) and x-ray diffraction. It was found that the structure of nano-phase powder is different from bulk NiTi alloy with bcc structure as target materials. When increasing the annealing temperature, a small fraction of the (Ni,Ti) type nanocrystal with the hexagonal structure was presented except target materials and Ni, and it is atomic occupation in random. Finally there were four Ti and two Ni atoms around central Ni atoms, and the bond length of Ni-Ti and Ni-Ni were 0.2462 nm and 0.2585 nm at 800°C annealed.

Keywords: NiTi nanocrystals, Phase transition

1. Introduction

The NiTi shape memory alloy (SMA) with an approximately equal atomic ratio is a kind of novel functional materials which has the ability to return to a previously defined shape and size when subjected to the appropriate thermal procedure. These materials can be plastically deformed at a relatively low temperature, and will return to their shapes prior to the deformation during exposure to a higher temperature. Actually the NiTi SMA is unique memory alloy materials with extensive applications (Hwang, C.M., et al., 1983; Ling, H.C. et al., 1980, 1981; Nishida, M., et al., 1986; Miyazaki, S., et al., 1988).

Until now, people have not known what the behavior of NiTi alloy will be when decreasing the grain size to nanometer. No reports have been published on the local structure of nanoscale NiTi alloy. On the other hand, determination of the atomic structure of nanoscale solids is very important for understanding the properties of nano-materials. In the past decades, a huge number of investigations on the characteristic and the microstructure of nano-materials have been presented using various methods of structural analysis. Among them, extended x-ray absorption fine structure (EXAFS) is a powerful tool for identifying the local structure around the absorbing atoms. In this paper, the NiTi SMA was chosen as a target material to prepare the NiTi nanocrystal, then the local structure around Ni atoms was studied using the combination of EXAFS and XRD.

2. Experiments

The raw nano-NiTi powder, with a particle size of 7 nm, was synthesized using DC sputtering on a dedicated apparatus, which was named as "glow discharge-condensation-in situ pressure", and set up by Institute of Solid State Physics, Chinese Academy of Sciences (Zhu, Y., 1994), then condensed, and finally shaped with a pressure of 1.5 GPa. The target materials is a bulk NiTi SMA with bcc structure. A series of samples with different particle size were prepared by annealing the raw powder in vacuum at

400, 600 and 800°C respectively. EXAFS measurements at the Ni K-edge were performed in the transmission mode at the EXAFS station on beamline 4W1B of the Beijing Synchrotron Radiation Facility (BSRF). The storage ring operated at 2.2 GeV and 40–50 mA. Data analysis was performed using the EXCURV92 program. X-ray diffraction measurements were performed at beamline 4B9A of BSRF. A x-ray diffractometer with the precision of 0.001 degree is the main equipment. The incident beam intensity was monitored with an ion chamber and the diffracted intensity was detected by NaI(Tl) scintillation detector. There were two slits of 0.5 mm on the light path, one was set at the entrance of the beam and the other was at the front of the detector. The incident focused and monochromatic x-ray beam was calibrated by the Cu K-edge (1.54 Å). The energy resolution $\Delta E/E$ was 4×10^{-4} .

3 Results and discussion

3.1 XRD

From transmission electron microscopy (TEM) experiments, it was found that the NiTi grains grow in size when the annealing temperature increases, and finally their particle size increases to about 20 nm by raising the temperature to 800°C (X. Ju et al., 1995).

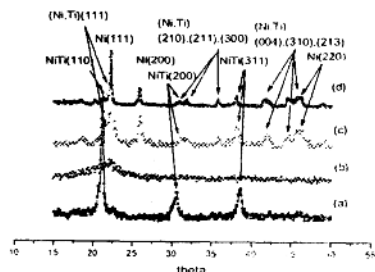


Fig. 1 X-ray diffraction patterns of nano-NiTi samples. (a) NiTi alloy; (b) as-grown NiTi powder; (c) annealing at 400°C; (d) annealing at 600°C

The as-grown NiTi powder was prepared by the DC sputtering method using NiTi SMA target with the bcc structure. Figure 1 shows the XRD pattern of the target material. Three strong peaks are attributed to (110), (200) and (211) as indicated in Fig. 1(a). Fig. 1(b) shows the diffraction pattern of the as-grown NiTi powder. There is a broad peak corresponding to non-crystalline materials. Figures 1(c) and (d) correspond to the samples obtained by annealing at 400 and 600°C respectively. The structure of these samples identified from the diffraction patterns is not the same as the bcc structure of the target material. At first, it can be exhibited a group of strong diffraction peaks of Ni with a cubic structure. As indicated in Fig. 1(c) and (d), the strongest peak is at $\theta=22.2^\circ$ for (111), the peaks at $\theta=25.6, 33.0$ and 46.4° are identified as the (200), (220) and (311) of Ni crystalline with a cubic structure. Meanwhile, it should be pointed out that two groups of weak peaks exist and are corresponding to target material and the (Ni,Ti) type alloy with hexagonal structure, which is atomic occupation in random. As indicated, the peak at $\theta=3.9^\circ$

Commercial polyethylene-terephthalate (PET) film from Japan with a thickness of $16\mu\text{m}$ was irradiated at the tandem accelerator of China Institute of Atomic Energy, Beijing, with sulfur ions (4.1MeV/amu) with a fluence of 3×10^8 ions per cm^2 . The ion irradiated PET film was UV irradiated for track sensitization. The film was then sensitized with ammonia water moreover. Etching was performed with a 0.5N NaOH aqueous solution at 73°C to produce membranes with a pore diameter of $0.2\mu\text{m}$. A 20nm gold layer was sputtered onto one side of the membrane serving as the working electrode. A $3\mu\text{m}$ nickel film was then electroplated on the gold surface of the membrane so that the electrode completely covered and sealed the pores of the membrane. Deposition of CdS into the pores of the membrane was carried out galvanostatically (current density = $2.0\text{mA}/\text{cm}^2$, time = 40min) in a solution that contained 0.055M CdCl_2 and 0.19M elemental sulfur dissolved in DMSO at 110°C . The solution was stirred with a magnetic stirrer during deposition. A film of CdS was also deposited on Al substrate under the same condition in order to produce the sample 1 for comparison. On the other hand, the samples 2, 3 were prepared at 125°C under different the current density, $3.0\text{mA}/\text{cm}^2$ and $5.0\text{mA}/\text{cm}^2$, respectively.

The scanning electron microscope (SEM) experiments for both nanowire array and films were carried out on Hitachi S-450 instrument operated at 20 kV and equipped with energy dispersive X-ray (EDX) fluorescence microanalysis in order to obtain morphological information and the atomic composition of the semiconductor samples. The sample of CdS nanowire array for the SEM was prepared by dissolving the membrane in a solution composed of KOH, water and ethanol at room temperature for a long time. The crystal structure of the samples was analyzed by a D/max-RB diffractometer with $\text{Cu K}\alpha$ radiation.

The sample of CdS nanowire array for optical experiments was prepared by removing the metal layer from the membrane by polishing. The samples of CdS films as contrast were removed from the Al substrate by attaching the exposed face of the CdS films to a transparent adhesive tape and then dissolving the Al substrate in a NaOH aqueous solution (6.8N). Absorption spectra were taken using a Beckman BU-600 spectrophotometer at room temperature. Photoluminescence spectra were measured with a PERKIN ELMER LS50B luminescence spectrometer.

3. RESULTS AND DISCUSSION

3.1. SEM and XRD

The images of CdS nanowire array and films are shown in Fig. 1. For the samples of CdS nanowire array, it is apparent that the deposited semiconductor fills the pores uniformly and continuously, which means the semiconductor faithfully reproduce the shape of the pores. It is also revealed that the nuclear track membrane suppresses the morphology with significant cracking, typical of electrodeposited CdS in DMSO⁴. Thus template restriction of the growth dimensions can improve the overall morphology of electrodeposited semiconductor materials. In addition, the sample 1 consists of granular structure with cracks; the samples 2 and 3 are close to the crystallites with holes. These indicate that the samples crystallize well at higher temperature. The semiquantitative analysis of CdS nanowire array by EDX gives a composition of $50.1\text{ at } \%$ Cd, $45.7\text{ at } \%$ S and $4.2\text{ at } \%$ Cl. For a comparison, the atomic composition of the films is similar to that of the nanowire array. But, the Cd content of the sample 3 is stoichiometric excess, about 2% , meanwhile, there is a trace of elemental Cl, $<4\%$.

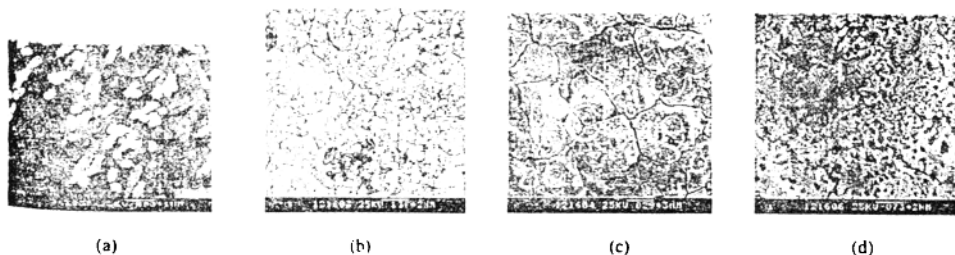


Fig 1. The SEM images of CdS nanowire array and films. (a) the nanowire array sample, 110°C , 2.0mA ; (b) the film sample 1, 110°C , 2.0mA ; (c) the film sample 2, 125°C , 3.0mA ; (d) the film sample 3, 125°C , 5.0mA

Preparation and photoluminescence of nanowire array and films of cadmium sulfide by electrodepositing in organic solvent

X. Ju¹, L. Q. Peng

BSRF, Institute of High Energy Physics, CAS, Beijing 100039, P. R. China

ABSTRACT

Nanowire array and film of cadmium sulfide were prepared by electroplating in organic solvent dimethyl sulfoxide with CdCl_2 and element sulfur under different temperature and current density. The UV-VIS absorption spectra show that increasing the electroplating temperature is benefit to forming perfect crystallites and the absorption peak under high electroplating temperature is ascribed to the excitonic transition. The formula of energy shift for the lowest several excitons is given and compared with the experiment. The photoluminescence spectrum consists of two parts: the first is produced by recombination of the defects and the second by recombination of excitons.

Keywords: CdS, nanowire array, electroplating

1. INTRODUCTION

The nature of semiconductor nanomaterials is situated between that of the corresponding molecules and bulks. The change of their physical and chemical properties is noticeable to follow their dimension¹. Semiconductor cadmium sulfide (CdS) is of the remarkable effect of quantum size. There are lots of experiments to investigate the relationship between the optical absorption, photoluminescence and the micro-crystallites size. It indicates that the features of the photoluminescence spectroscopy for CdS nano-crystallite, which grows in zeolite, polymer and glass, depends on the preparation of samples² and reflects the information on the impurity, defect and surface state³. Since A. S. Baranski etc. obtained the II-VI group semiconductor in organic solvents with the electrodepositing method⁴, a series of investigations on their preparation, behavior and applications such as solar cell have been carried out⁵. Generally, the CdS nano-crystalline preparing in chemical reaction at room temperature, sometimes with the annealing, is embraced by inert surface or embedded in the isolated materials. But, it is different that the CdS nano-crystalline is electrodeposited in organic solvent at higher temperature, which is of the metal-like multi-crystallite structure without the impurities.

On the other hand, template synthesis is an elegant chemical approach for the fabrication of nanowires and has attracted more and more attention. Arrays of metal^{6,8}, semiconductor⁷, conducting polymer⁹ nanowires and carbon nanotubes¹⁰ are obtained by electrodepositing or other methods in porous templates such as anodic aluminum oxide films and nuclear track membranes. Applications of these materials include arrays of electron field emitters¹¹, nanoelectrodes for electrochemical experiments¹², magnetic sensors based in the giant magnetoresistance effect¹³ and anisotropic optical filters¹⁴.

Although CdS nanowire arrays with diameter as small as 9nm have been fabricated in anodic aluminum oxide films with the oxide barrier layer separating the Al substrate and the porous aluminum oxide⁵, there is a main constraint in the experiments such as absorption spectra in order to separate CdS nanowire arrays from the Al substrate. However, the characterization of CdS nanowire arrays can be studied thoroughly if they are fabricated in nuclear track membranes. In this paper, we report the fabrication and optical characterization of CdS nanowires with a diameter of 200nm in nuclear track membranes and the corresponding films under the same or different conditions by electroplating in organic solvent dimethylsulfoxide (DMSO).

2. EXPERIMENTAL

¹ Correspondence: jux@ihep.ac.cn, Telephone: 86-10-68235998; Fax: 86-10-68186229

Commercial polyethylene-terephthalate (PET) film from Japan with a thickness of 16 μ m was irradiated at the tandem accelerator of China Institute of Atomic Energy, Beijing, with sulfur ions (4.1MeV/amu) with a fluence of 3×10^8 ions per cm^2 . The ion irradiated PET film was UV irradiated for track sensitization. The film was then sensitized with ammonia water moreover. Etching was performed with a 0.5N NaOH aqueous solution at 73°C to produce membranes with a pore diameter of 0.2 μ m. A 20nm gold layer was sputtered onto one side of the membrane serving as the working electrode. A 3 μ m nickel film was then electroplated on the gold surface of the membrane so that the electrode completely covered and sealed the pores of the membrane. Deposition of CdS into the pores of the membrane was carried out galvanostatically (current density = 2.0 mA/cm², time = 40 min) in a solution that contained 0.055M CdCl₂ and 0.19M elemental sulfur dissolved in DMSO at 110°C. The solution was stirred with a magnetic stirrer during deposition. A film of CdS was also deposited on Al substrate under the same condition in order to produce the sample 1 for comparison. On the other hand, the samples 2, 3 were prepared at 125°C under different the current density, 3.0mA/cm² and 5.0mA/cm², respectively.

The scanning electron microscope (SEM) experiments for both nanowire array and films were carried out on Hitachi S-450 instrument operated at 20 kV and equipped with energy dispersive X-ray (EDX) fluorescence microanalysis in order to obtain morphological information and the atomic composition of the semiconductor samples. The sample of CdS nanowire array for the SEM was prepared by dissolving the membrane in a solution composed of KOH, water and ethanol at room temperature for a long time. The crystal structure of the samples was analyzed by a D/max-RB diffractometer with Cu K α radiation.

The sample of CdS nanowire array for optical experiments was prepared by removing the metal layer from the membrane by polishing. The samples of CdS films as contrast were removed from the Al substrate by attaching the exposed face of the CdS films to a transparent adhesive tape and then dissolving the Al substrate in a NaOH aqueous solution (6.8N). Absorption spectra were taken using a Beckman BU-600 spectrophotometer at room temperature. Photoluminescence spectra were measured with a PERKIN ELMER LS50B luminescence spectrometer.

3. RESULTS AND DISCUSSION

3.1. SEM and XRD

The images of CdS nanowire array and films are shown in Fig. 1. For the samples of CdS nanowire array, it is apparent that the deposited semiconductor fills the pores uniformly and continuously, which means the semiconductor faithfully reproduce the shape of the pores. It is also revealed that the nuclear track membrane suppresses the morphology with significant cracking, typical of electrodeposited CdS in DMSO⁴. Thus template restriction of the growth dimensions can improve the overall morphology of electrodeposited semiconductor materials. In addition, the sample 1 consists of granular structure with cracks; the samples 2 and 3 are close to the crystallites with holes. These indicate that the samples crystallize well at higher temperature. The semiquantitative analysis of CdS nanowire array by EDX gives a composition of 50.1 at % Cd, 45.7 at % S and 4.2 at % Cl. For a comparison, the atomic composition of the films is similar to that of the nanowire array. But, the Cd content of the sample 3 is stoichiometric excess, about 2%, meanwhile, there is a trace of elemental Cl, <4%.

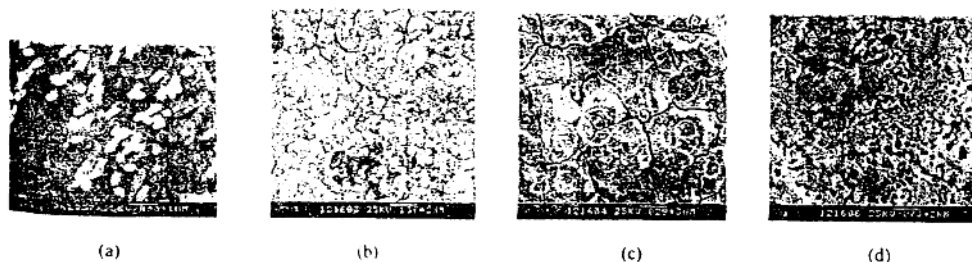


Fig 1. The SEM images of CdS nanowire array and films (a) the nanowire array sample, 110°C, 2.0mA; (b) the film sample 1, 110°C, 2.0mA; (c) the film sample 2, 125°C, 3.0mA; (d) the film sample 3, 125°C, 5.0mA

The x-ray diffraction peaks of the sample of CdS nanowire array and films could be assigned to the hexagonal greenockite phase CdS, Ni, Au and nuclear track membrane, without any trace of elemental Cd or S. Additionally, in the calculation of the crystallite size, the effect of the non-uniform stress in CdS should be removed¹⁵. Analysis of the width of the peaks using the Debye-Scherrer formula indicates that the crystallite size of CdS in the nanowire array sample is on the order of 10-20nm when neglecting the stress effect, similar to those in CdS films¹⁶. Here, as reference, the average crystallite size of the sample 1 was estimated to be about 20 nm. Similarly, that of both the sample 2 and 3 is about 10nm.

3.2. UV-VIS spectra

The absorption spectrum of CdS nanowire array and films are shown in Fig.2. The optical band gap of all samples is 515.5nm (2.40eV), and corresponds well to that of CdS. All of this together with the available data on the electrodeposition of CdS from DMSO^{4,15,16} makes us confident that the deposited material in nuclear track membrane is n-CdS doped with Cd and Cl. For CdS nanowire array, the most striking feature is that there is a well-developed maximum at the wavelength of 690 nm, located in lower energy side of the onset of absorption. The onset of absorption shows no shift to that of the CdS films¹⁶. On the other hand, the samples 2 and 3 are of distinguishing peak of exciton at higher side of the onset of absorption⁷. The positions of the absorption of both samples are at 485.5nm with a FWHM of 0.35eV and 489.7nm with a FWHM of 0.2eV, respectively. Moreover, there is a shoulder at 459nm for the sample 3. Compared to colloid CdS⁷, the crystallite size of the samples 2 and 3 is about 10nm, and that of the sample 1 is little bigger and close to the estimated value by XRD.

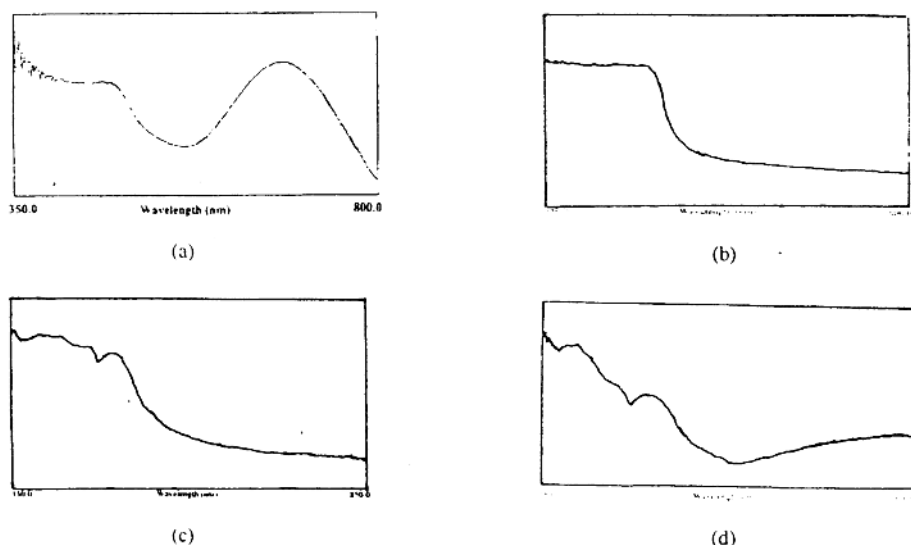


Fig.2. The absorption spectra of sample of CdS nanowire array and films. (a) the nanowire array sample; (b) the film sample 1; (c) the film sample 2; (d) the film sample 3

3.3. Photoluminescence spectra

The photoluminescence spectra of the CdS nanowire array and the film are shown in Fig.3, accompanying with the exciting spectrum of the sample 1 since that of all samples is almost identical. The spectrum of the CdS sample 1 shows three broad emission bands that have three major peaks at 530, 590 and 660nm, respectively. For the band at 530nm, it is 0.6eV below the onset of absorption and not occurred in CdS nano-crystallite prepared in chemical reaction. Considering the existence of Cl ion in the electrodeposited CdS films, which acts as a shallow donor and contributes to the very high electron density¹⁵, it is ascribed to originate from the recombination of the energy level of the donor. The

spectrum of the CdS nanowire array shows similar structure except for indistinct peaks at 530nm and 590nm due to low signal to noise ratio. Both the 590 and 660nm broad bands can be observed in photoluminescence spectra of CdS clusters and attributed to Cd atoms and sulfur vacancy, respectively^{3, 17}. From the analysis of atomic composition, Cd atoms and sulfur vacancy should also exist in the samples of CdS nanowire array and films. Thus we assign the 590nm and 660nm bands to Cd atoms and sulfur vacancy respectively. For sample 2 and 3, there are two narrow bands at 486 and 460nm with a FWHM of 0.04eV, which corresponds to that of the absorption spectra and is from the recombination of the bound-exciton.

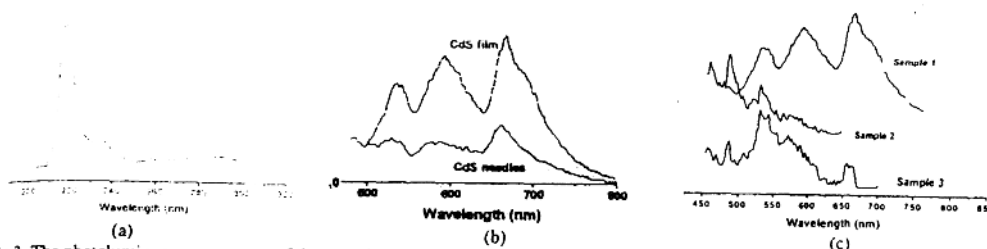


Fig.3. The photoluminescence spectra of the samples of CdS nanowire array and films. (a) the exciting spectrum of film sample 1; (b) the nanowire array sample and the film sample 1; (c) the film sample 1-3

Because of the size effect in nanocrystalline, the exciton is bound with higher energy and intensity, so the absorption of exciton can be presented at room temperature. Under the approximation of effective mass, the relationship between energy shift of the lowest energy exciton, ΔE , and radius, R , is as follows:

$$\Delta E = \frac{\hbar^2 \pi^2}{2R^2} \left[\frac{1}{m_e} + \frac{1}{m_h} \right] - \frac{1.786e^2}{\epsilon \cdot R} - 0.248 E_{Ry}^*$$

in which the first term is the kinetic energy of the minimum quantization in rectangular potential well; m_e and m_h is the mass of electron and hole, respectively. The second term is the Coulomb potential between electron and hole. ϵ is dielectric constant. The third term is the correlation energy, and very small in common. Generally, there is a big difference between the formula and experiments when R is small, but the calculation is consistent with experiments in the region of 3-4nm^{18, 19}. Supposed that $m_e=0.165m$ and $m_h=0.98m$ (m : the mass of electron) and $\epsilon=5.5^3$, the calculated radius with this formula is 4nm at the lowest exciton energy, 498nm, and very close to results from XRD experiments. Regarding the common expression of the quantization energy of particle in rectangular potential well²⁰, ΔE can be shown:

$$\Delta E = \frac{\hbar^2 k_{l,m}^2}{2R^2} \left[\frac{1}{m_e} + \frac{1}{m_h} \right] - \frac{1.786e^2}{\epsilon \cdot R} - 0.248 E_{Ry}^*$$

in which the $k_{l,m}$ is quantum number, as known, $k_{1,0}=3.14$, $k_{1,1}=4.49$, $k_{1,2}=5.76$. The calculated second lowest energy of exciton is 457nm with a radius of 4nm, and in accordance with our experimental value, 460nm.

There is no absorption of exciton for the sample 1. This is because its size is bigger and the intensity is weaker^{2, 21}. On the other hand, it may concern the imperfect growth of crystallites at lower temperature in electrodeposition process. In our experiment, the onset of absorption of the CdS films, prepared the materials at 100°C under different current density, shifts blue 2.60eV without absorption of exciton, which indicates the electrodeposition temperature is of a great impact on the optical properties of CdS nanomaterials. Additionally, when the amorphous CdS, electrodeposition at room temperature, is annealed at 600°C, the crystallization is still worse than that at 100°C, which means that the electrodeposition temperature is more important than the annealing one. Compared to results of reference 4, the photoluminescence of the samples 2 and 3 are stronger with the same crystallite size. It may attribute that different electrodeposition temperature results in different degree of crystallization. The photoluminescence of sample 2 is stronger than that of sample 3, which shows that the crystallization of semiconductor is better when electrodeposition with a weaker current

density at the same temperature²². Consequently, the change of photoluminescence is also related to the perfection of crystallite.

As described above, there are same native defects and impurity defects in the sample of CdS nanowire array and CdS film sample, which eliminates the possibility that the absorption peak in Fig.2 is ascribed to the defects. Additionally, there is no sharp emission band with peak at 690nm in the photoluminescence spectrum of the sample of CdS nanowire array, which eliminates the bound-exciton as the possible mechanism for the absorption peak. Considering that there are a number of interface states between the CdS nanowire array and the membrane pores, we therefore assign it to the interface states transition. This is also supported by the following facts: the typical value of semiconductor surface potential 0.5V²³ is near the 0.6eV difference value between the absorption peak and the onset of absorption; the recombination by surface states is a radiationless relaxation process.

4. CONCLUSION

It can be concluded that (1) CdS nanowire array with a diameter of 200nm have been fabricated by electrochemical deposition in nuclear track membrane. An intense absorption peak of the CdS nanowire array was observed and it could be assigned to transition of the interface states; (2) increasing the electrodeposition temperature is favor to grow nanocrystallites with perfect structure, and results in the absorption of exciton; (3) the formula for the secondary lowest energy shift is given, and consistent with our experiments; (4) the spectra of photoluminescence is composed of bands from the recombination of impurity, defect etc., in which the bands from the stronger recombination of exciton corresponds to that of the bound-exciton. Finally, their intensity is related to the perfection of crystallite.

REFERENCES

1. A. P. Alivisatos, "Semiconductor Clusters, Nanocrystals, and Quantum Dots," *Science*, **27**, pp. 1933-1937, 1996
2. T. Vossmeier, L. Katsikas, M. Giersig, I. G. Popovic, K. Diesner, A. Chemseddine, A. Eychmuller, H. Weller, "CdS nanoclusters: Synthesis, characterization, size-dependent oscillator strength, temperature shift of the excitonic transition energy, and reversible absorbance shift," *J. Phys. Chem.* **98**, pp. 7665-7673, 1994
3. Y. Wang and N. Herron, "Photoluminescence and relaxation dynamics of CdS superclusters in zeolites," *J. Phys. Chem.* **92**, pp. 4988-4994, 1988
4. A. S. Baranski, W. R. Fawcett, A. C. McDonald and R. M. de Nobrega, "The structural characterization of Cadmium Sulfide films grown by cathodic electrodeposition," *J. Electrochem. Soc.* **128**, pp. 963-968, 1981
5. D. Routkevitch, T. Bigioni, M. Moskovits and J. M. Xu, "Electrochemical fabrication of CdS nanowire arrays in porous anodic aluminum oxide," *J. Phys. Chem.* **100**, pp. 14037-14047, 1996
6. C. R. Martin, "Nanomaterials: a membrane-based synthetic approach," *Science*, **266**, pp. 1961-1966, 1994
7. L. Wang, K. Yu-Zhang, A. Metrot, P. Bonhomme and M. Troyon, "TEM study of electrodeposited Ni/Cu multilayers in the form of nanowires," *Thin Solid Film*, **288**, pp. 86-89, 1996
8. C. Schonenberger, B. M. I. van der Zande, L. G. J. Fokkink, M. Henney, C. Schmidt, M. Krugel, A. Bachtold, R. Huber, H. Birk and U. Staufer, "Template synthesis of nanowires in porous polycarbonate membranes: electrochemistry and morphology," *J. Phys. Chem.* **B101**, pp. 5497-5505, 1997
9. L. Piroux, S. Dubois and S. Demoustier-Champagne, "Template synthesis of nanoscale materials using the membrane porosity," *Nucl. Instrum. Meth.* **B131**, pp. 357-363, 1997
10. W. Z. Li, S. S. Xie, L. X. Qian, B. H. Chang, B. S. Zhou, W. Y. Zhou, R. A. Zhao and G. Wang, "Large scale synthesis of aligned carbon nanotubes," *Science*, **274**, pp. 1701-1703, 1996
11. W. A. de Heer, A. Chatelain and D. Ugarte, "A carbon nanotube field-emission electron source," *Science*, **270**, pp. 1179-1180, 1995
12. V. P. Menon and C. R. Martin, "Fabrication and evaluation of nanoelectrode ensembles," *Anal. Chem.* **67**, pp. 1920-1928, 1995
13. L. Piroux, J. M. George, J. F. Despre, C. Leroy, E. Ferain, R. Legras, K. Punadjela and A. Fert, "Giant magnetoresistance in magnetic multilayered nanowires," *Appl. Phys. Lett.* **65**, pp. 2484-2486, 1994
14. C. A. Foss, G. L. Hornyak, J. A. Stockert and C. R. Martin, "Template synthesis of nanoscopic gold particles: optical spectra and the effects of particle size and shape," *J. Phys. Chem.* **98**, pp. 2963-2971, 1994
15. A. S. Baranski, M. S. Bennett and W. R. Fawcett, "The physical properties of CdS thin films electrodeposited from aqueous diethylene glycol solution," *J. Appl. Phys.* **54**, pp. 6390-6394, 1983

16. E. Fatas, P. Herrasti, F. Arjona, E. G. Camarero and J. A. Medina, "Electrodepositing and characterization of CdS thin films on stainless steel and tin oxide substrates," *Electrochimica Acta*, **32**, pp. 139-148, 1987
17. J. J. Ramsden, S. E. Webber and M. Gratzel, "Luminescence of colloidal CdS particles in acetonitrile and acetonitrile/water mixtures," *J. Phys. Chem.* **89**, pp. 2740-2743, 1985
18. P. E. Lippens and M. Lannoo, "Calculation of the band gap for small CdS and ZnS crystallites," *Phys. Rev.* **B39**, pp. 10935-10942, 1989
19. Y. Wang and N. Herron, "Quantum size effects on the exciton energy of CdS clusters," *Phys. Rev.* **B42**, pp. 7253-7255, 1990
20. J. X. Fang and D. Lu, *Solid State Physics*, Scientific and Technological Press, Shanghai, 1981
21. Y. Kayanuma, "Quantum-size effects of interacting electrons and holes in semiconductor microcrystals with spherical shape," *Phys. Rev.* **B38**, pp. 9797-9805, 1988
22. A. C. Rastogi and K. S. Balakrishnan, "Monocrystalline CdTe Thin Films by Electrochemical Deposition From Aprotic Electrolytes," *J. Electrochem. Soc.* **136**, pp. 1502-1505, 1989
23. K. Seeger, *Semiconductor Physics*, Springer-Verlag, Wien, 1973

Evidence for change of the interfacially local structure of titanium oxide/bis[(4,4'-carboxy-2,2'-bipyridine)(thiocyanato)] ruthenium nanocomposite[†]

X. Ju,^{1*} J. Zhang,¹ K. W. Wu,² Y. J. Hou,² P. H. Xie² and B. W. Zhang²

¹Institute of High Energy Physics, Chinese Academy of Sciences, Beijing 100039, P.R. China

²Institute of Photography, Chinese Academy of Sciences, Beijing 100101, P.R. China

Received 23 October 2000; Revised 7 December 2000; Accepted 9 January 2001

Titanium oxide/bis[(4,4'-carboxy-2,2'-bipyridine)(thiocyanato)]ruthenium (*cis*-(NCS)₂RuL₂) nanocomposites were prepared by the self-assembly method. In this system, their interfacially local structures were probed by x-ray absorption spectroscopy (XAS) and the Ti–O interatomic distance and the coordination number of the O atoms around the Ti central atoms were extracted. Compared with TiO₂ nanoparticles, the Ti local structure in the nanocomposite was changed, which is responsible for binding *cis*-(NCS)₂RuL₂ to the surface of TiO₂ nanoparticles. Copyright © 2001 John Wiley & Sons, Ltd.

KEYWORDS: XAS; TiO₂/*cis*-(NCS)₂RuL₂ nanocomposite

INTRODUCTION

A new type of photovoltaic cell was reported recently based on spectral sensitization of thin nanocrystalline TiO₂ (anatase) films by ruthenium polypyridine complex chromophores.¹ Generally, interfacial electron transfer from photoexcited states of the chromophore into the conduction bands of the semiconductor depends on a number of factors. The structural and electronic properties of the interface are very important² but they are not completely clear. The techniques of x-ray absorption near-edge structure (XANES) and extended x-ray absorption spectroscopy (EXAFS)—together called x-ray absorption fine structure (XAFS)—are atom specific and capable of probing the short-to-medium range structure around an imbedded or absorbing atom,³ which can provide the structural origin of the unique photoelectronic property of the nanocomposite. In this work, we prepare a TiO₂/bis[(4,4'-carboxy-2,2'-bipyridine)(thiocyanato)]ruthenium (*cis*-(NCS)₂RuL₂) nanocomposite by the self-assembled method, and present our recent XAS study on the Ti K-edge on TiO₂ nanoparticles of 10–20 nm without and with an assembly of *cis*-(NCS)₂RuL₂. Surface distortion of the Ti in the TiO₂ nanoparticles and the interfacial interaction between TiO₂ and *cis*-(NCS)₂RuL₂ are discussed.

EXPERIMENTAL

The TiO₂ film was prepared by casting 11% TiO₂ nanoparticles of size 10–20 nm on the glass substrate and heat treating

at 450 °C for 30 min. The TiO₂/*cis*-(NCS)₂RuL₂ nanocomposite was obtained by dipping the TiO₂ film into the *cis*-(NCS)₂RuL₂ ethanol solution for 24 h⁵ and then drying for 2 days. The XAS spectra at the Ti K-edge were measured in transmission mode by using synchrotron radiation with a Si(111) double-crystal monochromator on the EXAFS station at the 4WIB beamline of Beijing Synchrotron Radiation Facility (BSRF). The storage ring was operated at 2.2 GeV with a beam current of ~80 mA. The energy resolution was 1.5 eV for the near-edge structure and ~3.0 eV for the EXAFS. Data analysis were performed in the EXCURV88 program.

RESULTS

X-ray absorption near-edge structure

The XANES spectra at the Ti K-edge of bulk TiO₂, TiO₂ nanoparticles and TiO₂/*cis*-(NCS)₂RuL₂ nanocomposites are shown in Fig. 1. As is known, the XANES spectrum contains several well-defined pre-edge peaks that are related to the local structure surrounding Ti atoms. For bulk TiO₂ (anatase), it exhibits three small pre-edge peaks (A₁, A₂, A₃) that are assigned respectively to transitions from the 1s core level of Ti to 1t_{1g}, 2t_{2g} and 3e_g molecular orbitals.⁶ On the other hand, the intensities of these pre-edge features are a strong function of the distortion of the oxygen octahedron around the central absorbing Ti atom. For TiO₂ nanoparticles, an increase in the intensity of the A₂ peak is observed, indicating an increasing distortion from the oxygen octahedron that may result from the surface effect of TiO₂ nanoparticles.⁶ However, there is very little effect of the *cis*-(NCS)₂RuL₂ assembly on the XANES spectrum for TiO₂ nanoparticles.

*Correspondence to: X. Ju, Institute of High Energy Physics, Chinese Academy of Sciences, Beijing 100039, P.R. China.
E-mail: jux@alpha02.ihep.ac.cn

[†]Paper presented at APSIAC 2000: Asia–Pacific Surface and Interface Analysis Conference, 23–26 October 2000, Beijing, China.

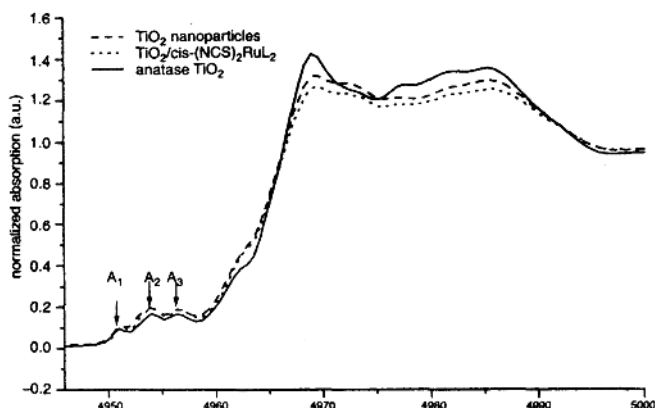


Figure 1. The XANES spectra at the TiK edge of bulk TiO_2 , TiO_2 nanoparticles and $\text{TiO}_2/\text{cis}-(\text{NCS})_2\text{RuL}_2$ nanocomposites.

Extended x-ray absorption fine structure

The radial distribution functions (RDF) of TiO_2 nanoparticles and the $\text{TiO}_2/\text{cis}-(\text{NCS})_2\text{RuL}_2$ nanocomposite are shown in Fig. 2. The fitting results are listed in Table 1, along with the standard crystalline TiO_2 in anatase phase.

For all samples, the first-shell Ti–O peak in the Fourier transform EXAFS spectra was fitted on a two-subshell model.

The bond lengths r_1 and r_2 of two Ti–O subshells of TiO_2 nanoparticles and $\text{TiO}_2/\text{cis}-(\text{NCS})_2\text{RuL}_2$ nanocomposite are different from that of the reference standard. It is well known that the structure of nanomaterials is relaxed from the perfect crystal structure to the local structure with amorphous features. For most nanomaterials, the interatomic distance become shorter as the particle size decreases, but the bond

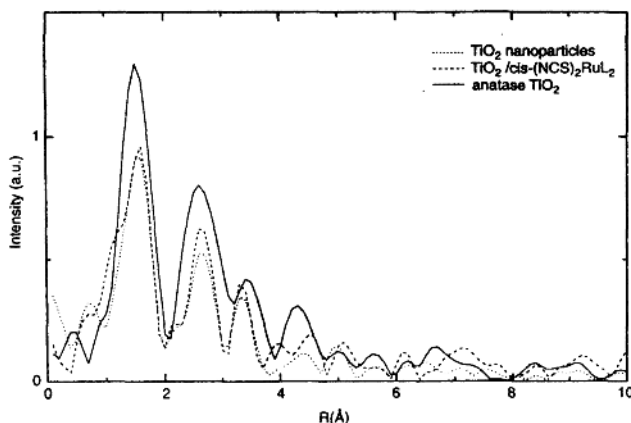


Figure 2. The EXAFS spectra of bulk TiO_2 , TiO_2 nanoparticles and $\text{TiO}_2/\text{cis}-(\text{NCS})_2\text{RuL}_2$ nanocomposites.

Table 1. Fitting of the EXAFS parameters with EXCURV88

Sample	E_0	$r_1(\text{nm})$	$r_2(\text{nm})$	n_1	n_2	a_1	a_2
TiO_2 (anatase) ^a	8.479	1.906	1.936	4.0	2.0	—	—
TiO_2 nanoparticles	12.87	1.880	1.909	4.0	1.6	0.02026	0.01189
$\text{TiO}_2/\text{cis}-(\text{NCS})_2\text{RuL}_2$	11.94	1.857	1.901	2.7	2.2	0.01097	0.00972

^a The structural data were extracted from the PDF cards.

length of the first subshell of the $\text{TiO}_2/\text{cis}-(\text{NCS})_2\text{RuL}_2$ nanocomposite has an observable change compared with that of TiO_2 nanoparticles.

From the point of view of atomic coordination, the coordination numbers n_1 and n_2 of the O atoms around the Ti central atoms in the TiO_2 nanoparticles are 4.0 and 1.6, which is a little less than those of the reference standard ($n_1 = 4.0$, $n_2 = 2.0$). Actually, this is consistent with the properties of the local structure of nanomaterials, because the particle size of nanoparticles is small and results in an incomplete atomic coordination of the surface atoms.⁴ For the $\text{TiO}_2/\text{cis}-(\text{NCS})_2\text{RuL}_2$ nanocomposite, the corresponding coordination numbers are 2.7 and 2.2. This reveals that the Ti local structure is reconstructed when $\text{cis}-(\text{NCS})_2\text{RuL}_2$ is organized on the surface of the TiO_2 nanoparticles.

DISCUSSION

It should be pointed out that the above phenomena result from the assembly $\text{cis}-(\text{NCS})_2\text{RuL}_2$ on the surface of the TiO_2 nanoparticles, which can be attributed to the COOH groups in dye molecules coordinating to the Ti atoms of TiO_2 nanoparticles. In general, it is easier to form a complex of Ti and COOH on a surface,⁶ which would result in reconstruction of the Ti local structure. Therefore, compared with TiO_2 nanoparticles, the coordination number of the first subshell decreases and the bond length reduces⁷ in the nanocomposite. Finally, the Debye-Waller factors a_1 and a_2 in Table 1 can describe the degree of disorder of the materials. It is found that the $\text{TiO}_2/\text{cis}-(\text{NCS})_2\text{RuL}_2$

nanocomposite tends to have smaller values of such factors. As mentioned above, the COOH groups in the dye molecules are coordinated with the Ti atoms of the TiO_2 nanoparticles, and the complex relationship made the second subshell of the Ti-O full, which results in a modification and a smoothing of the surface of the TiO_2 nanoparticles.

CONCLUSION

In the composites studied here, $\text{cis}-(\text{NCS})_2\text{RuL}_2$ is assembled onto TiO_2 nanoparticles. The COOH groups in dye molecules can be coordinated with the Ti atoms on the surface of TiO_2 nanoparticles, which is expected to modify significantly the local structure of the TiO_2 nanoparticles. This study provides structural evidence for the interfacial property of the nanocomposites and acts as a guide for the rational design of electronic-optical materials.

REFERENCES

1. Braginsky L, Shklover VJ. *Solid. State Commun.* 1998; 105: 701.
2. Shklover V, Ovchinnikov YE, Braginsky LS, Zakeeruddin SM, Gratzel M. *Chem. Mater.* 1998; 10: 2533.
3. Iwasawa Y. *X-ray Absorption Fine Structure for Catalysts and Surfaces*. World Scientific: New Jersey, 1996.
4. Luca V, Djajanti S, Howe RF. *J. Phys. Chem. B* 1998; 102: 10650.
5. Nazeeruddin MK, Kay A, Rodicio J, Humphrey-Baker R, Muller E, Liska P, Vlachopoulos N, Gratzel M. *J. Am. Chem. Soc.* 1993; 115: 6382.
6. Zhang J, Ju X, Wang BJ, Li QS, Hu TD, Liu T. *Synth. Met.* 2001; 118: 181.
7. Chen LX, Rajh TJ, Jager W, Nedeljkovic J, Thurnauer MC. *J. Synchr. Radiat.* 1999; 6: 445.

机械球磨硒非晶化的 XAFS 研究

刘 涛, 吴自玉, 胡天斗, 张 静, 谢亚宁

(中科院高能物理所同步辐射室, 北京 100039)

赵永好, 卢 柯

(中科院金属所快速凝固与非平衡实验室, 沈阳 110016)

摘要:利用低温 EXAFS 和 XANES 方法研究了晶态 Se 在机械球磨过程中的结构变化。结果显示在球磨过程中引入链状分子间的中程无序, 破坏了分子间的结合, 而分子内 Se 原子以共价键结合, 不易被打破。

关键词:硒; 扩展 X-射线吸收精细结构谱; X-射线近边吸收谱; 机械球磨; 非晶

中图分类号: TG111

文献标识码: A

引言

硒不仅是对人体起重要作用的一种微量元素, 亦是静电复印、光电技术、半导体器件应用方面的重要组成部分。由于其独特的环状和链状结构, 也是理论和实验结构研究的重要材料^[1,2]。高能球磨法也称机械合金化是一种合成材料新工艺, 已成功制备出纳米晶纯金属、不互溶体系固溶体纳米晶、非晶合金、纳米金属间化合物及纳米金属-陶瓷复合材料等^[3]。

研究表明^[4], 经过一定时间的球磨, 可导致硒的非晶化。球磨过程产生大量的位错、晶界等结构缺陷是导致非晶化的原因。以往的研究多集中于合金、金属和类金属组分, 对以共价键结合的体系则涉及很少。由于硒具有与某些聚合物和生物分子类似的结构特征, 研究其机械球磨过程的结构变化, 可望对这类材料的结构和性能有更深入一步的了解。本文利用 EXAFS 和 XANES 方法对晶态 Se 在机械球磨过程的局域结构变化进行研究。

1 实验过程

X 射线衍射表明晶体硒为螺旋状三方晶系。将晶体硒粉末在机械球磨机内球磨, 氩气保护。将不同球磨阶段(球磨 40、120、250 min)的硒取出, 在粉末 X 射线衍射仪上测量衍射谱, 结果表明 250 min 以后样品已完全非晶化, 衍射结果见文献^[4]。硒的 K 边 EXAFS 测量在 BSRF 的 4W1B 光束线上, 在低温(77K)下以透射方式进行, 束流强度为 60~80 mA, EXAFS 数

• 收稿日期: 2000-11-20

基金项目: 中科院金属研究所快速凝固与非平衡实验室开放基金资助项目

作者简介: 刘涛, 男, 1966 年生, 副研究员。